

An atomic level analysis of conductivity and strength in poly(ethylene oxide) sulfonic acid-based solid polymer electrolytes

M. Grujicic^{a,*}, K.M. Chittajallu^a, G. Cao^a, W.N. Roy^b

^a Department of Mechanical Engineering, Program in Materials Science and Engineering, Clemson University, 241 Engineering Innovation Building, Clemson, SC 29634-0921, USA

^b Army Research Laboratory—Processing and Properties Branch, Aberdeen, Proving Ground, MD 21005-5069, USA

Received 27 February 2004; received in revised form 13 November 2004; accepted 21 November 2004

Abstract

The structure, ionic conductivity and strength of poly(ethylene oxide) (PEO) sulfonic acid-based solid polymer electrolytes with various contents of the PEO polymer are analyzed using molecular dynamics simulations. To quantify the electrolyte structure, comprehensive coordination and dimensional analyses are carried out. Ionic conductivity is determined by computing the Einstein-diffusion based conductivity for all ionic particles in the system. The strength of the electrolyte is quantified by carrying out a set of molecular simulations of the uniaxial deformation process under constant stress-rate conditions. The results obtained indicate that increased hydration improves the ionic conductivity, but degrades the strength in solid polymer electrolytes at hand. In addition, it appears that there is an optimal level of the PEO polymer content in these materials, which at the same hydration level, yields the best combination of ionic conductivity and strength.

© 2004 Elsevier B.V. All rights reserved.

Keywords: Solid polymer electrolytes; Ionic conductivity

1. Introduction

Over the last two decades, solid polymer electrolytes have been the subject of intense investigation due to their wide-range use as non-corrosive solid electrolytes in various electrochemical applications, electronic equipments, medical devices and in fuel cells for electrical and hybrid vehicles [1–5]. A comprehensive review of the synthesis, properties and applications of the proton-conducting solid polymer electrolytes can be found in Refs. [6,7].

In a comprehensive study, Herranen et al. [8] carried out synthesis and testing of a promising class of solid proton-conducting polymer electrolytes based on the poly(ethylene oxide) (PEO) with sulfonic acid end groups. These oligomeric electrolytes, referred to as the PEO sulfonic acids, are embedded in a high molecular weight PEO

matrix to obtain mechanically stable electrolyte membranes with ionic conductivities as high as 1.5 mS/cm. The molecular structure and the interactions between the molecules and the charge carriers were characterized using thermal analysis, impedance spectroscopy, NMR and IR spectroscopy [8].

The development of new materials via purely experimental means is a time-consuming and costly proposition. This is particularly true in the case of solid polymer electrolytes, since the mechanisms controlling various properties of these materials (primarily ionic conductivity, hydration behavior, osmosis, etc.) are not well understood and, hence, offer very little guidance to the material design process. Fortunately, a rapid increase in the computational resources, and the development of new highly efficient software packages combined with parallel advances in the experimental materials characterization tools now offer new opportunities for obtaining an insight into the atomic-level structure and mechanisms in these materials.

* Corresponding author. Tel.: +1 864 656 5639; fax: +1 864 656 4435.
E-mail address: mica.grujicic@ces.clemson.edu (M. Grujicic).

At present, there is a great need for solid polymeric electrolytes with an ionic conductivity in a mS/cm range, at temperatures around 100 °C. Among such solid electrolytes those which are proton-conducting are of particular importance due to their potential use as membranes in the polymer electrolyte membrane (PEM) fuel cells. Despite a significant research, which was devoted to understanding conductivity in proton-conducting polymers, the underlying mechanism of this process is still not well understood. It is generally accepted that there are two major contributions to the proton-conductivity in solid polymeric electrolytes in the presence of water: (a) diffusion of individual protons (or more precisely hydronium ions, H_3O^+) through the polymer electrolyte medium and (b) a proton hopping process within which protons combine with the water molecules to form hydronium ions and subsequently hop from these hydronium ions to the surrounding water molecules [9]. While the proton/hydronium diffusion mechanism can be studied using classical molecular dynamics simulations, and the corresponding value of the diffusion coefficient calculated from the simulation results, an explicit treatment of the proton hopping process entails the use of a quantum mechanical approach. Consequently, the proton hopping mechanism can be studied only in relatively small computational systems consisting of few tens of particles and, hence, the contribution of proton hopping to the overall proton transfer process in macroscopic systems may not be properly assessed.

In a series of papers, Ennari et al. [10–17] proposed a new approach to dealing with the proton hopping mechanism. Within this approach, a new particle named proton has been created and assigned the mass and the charge of a standard proton. However, the van der Waals radius of this particle has been derived from the condensed-phase properties of polymers containing highly polarized hydrogen (e.g. water or methanol). Consequently, the new particle can react with the surrounding molecules via strong Coulomb electrostatic forces and, hence, jump from one water molecule to the other. In this way, molecular dynamics simulations can be used to assess the contribution of the proton hopping mechanism to the proton transport in solid polymeric electrolytes. However, it should be noted that while the approach proposed by Ennari et al. [10–17] is capable of mimicking the proton hopping mechanism, it does not represent the true proton hopping process in which chemical bonds are broken within the hydronium molecules and generated within the water molecules. Nevertheless, the approach of Ennari et al. [10–17] offers a good first step toward dealing with a very complex problem, and since it yields diffusivity values comparable to their experimental parts [10–17], it is adopted in the present work.

The objective of the present work is to extend the approach of Ennari et al. [10–17] in order to explore the trade-off between a hydration-induced increase in ionic conductivity in the PEO sulfonic acid-based solid polymer electrolytes and the accompanied decrease in the material strength. When these solid polymer electrolytes are used in electrochemical

membrane applications, they must generally meet requirements pertaining to both the levels of their ionic conductivity and their strength.

The organization of the paper is as follows: details of the computer simulation procedure and the methods employed to analyze materials microstructure and properties of the material studied in the present work are overviewed in Section 2. The main results obtained in the present work are presented and discussed in Section 3. The key conclusions resulted from the present study are summarized in Section 4.

2. Computational procedure

2.1. Constituents

In all the calculations carried out in the present work, the following constituents are used: (a) PEO molecules based on a $(\text{CH}_2\text{CH}_2\text{O})$ repeat unit; (b) PEO sulfonic acid dianions with a formula $^-\text{O}_3\text{SCH}_2\text{CH}_2\text{CH}_2\text{O}(\text{CH}_2\text{CH}_2\text{O})_4\text{CH}_2\text{CH}_2\text{CH}_2\text{SO}_3^-$ and a molecular weight, $M_w = 436$; (c) water molecules (H_2O); (d) hydronium ions (H_3O^+); (e) protons (H^+). A schematic of these constituents and the charges of their atoms are displayed in Fig. 1.

2.2. Construction of the computational cells

To explore the effect of the PEO polymer content on ionic-transport and mechanical properties of PEO sulfonic acid-based solid electrolytes at the same weight-percent level of water, three (cubic) cells are constructed.

Each of the three cells contains four PEO sulfonic acid dianions with a formula, $^-\text{O}_3\text{SCH}_2\text{CH}_2\text{CH}_2\text{O}(\text{CH}_2\text{CH}_2\text{O})_4\text{CH}_2\text{CH}_2\text{CH}_2\text{SO}_3^-$ (molecular weight, $M_w = 436$), four (H^+) protons and four (H_3O^+) hydronium ions. To explore the effect of the PEO polymer content, the three cells contained one PEO molecule with the degree of polymerization: of 40 (Cell A), 60 (Cell B) and 80 (Cell C). To attain a fixed 40 wt.% of water, the three cells are also assigned 80, 111 and 142 water molecules, respectively. The edge lengths of the three unit cells are next adjusted to minimize the potential energy in each case. This procedure resulted in the following material densities: 0.90, 0.96 and 1.04 g/cm³ for the three cells, respectively. Furthermore, for each type of cells, 50 configurations are constructed.

In the present work, the structure and properties of PEO sulfonic acid-based electrolytes is studied using a larger number of initial configurations and relatively short runs (1000 ps). This is done, because it was observed that the starting structures generated by the Amorphous Cell Builder do not change substantially during longer runs. Hence, better statistics is expected from a larger number of short runs than from fewer long runs. In each case, the final properties are calculated using only the trajectory results from the last 200 ps.

Individual constituent molecules (e.g. PEO, H_3O^+ , etc.) are constructed using the Accelrys' software package

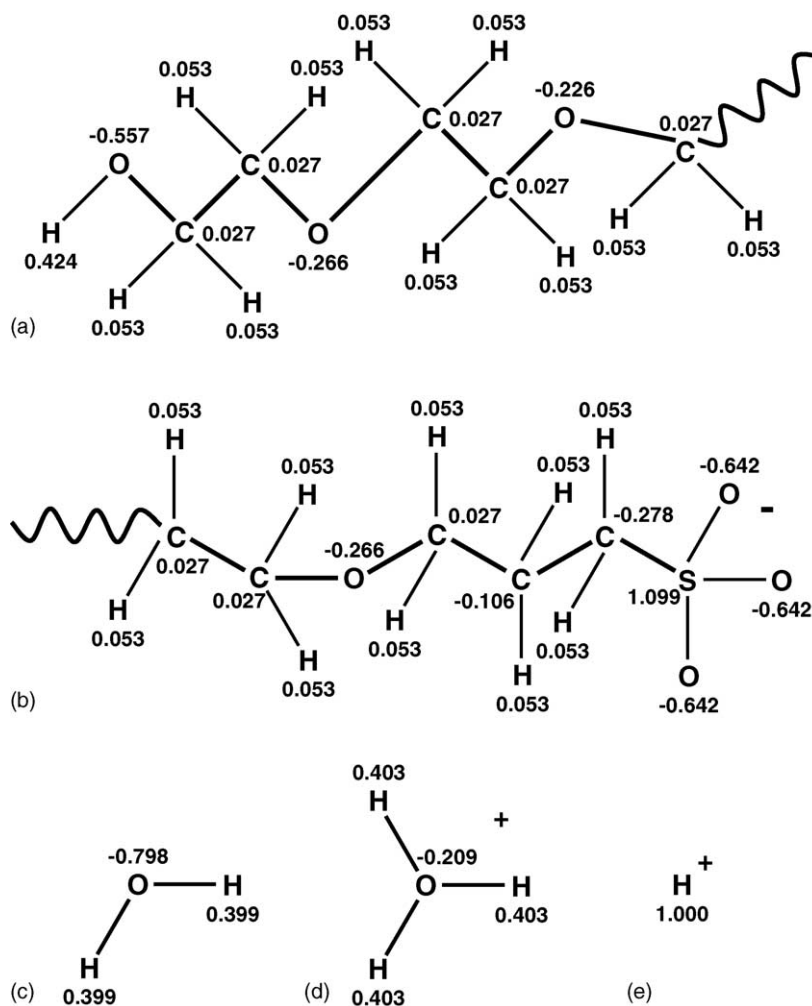


Fig. 1. Partial charges for the atoms in: (a) PEO; (b) PEO sulfonic acid dianion; (c) water; (d) hydronium; (e) proton.

Materials Visualizer [18], while the three cells containing the constituents described above are constructed using the Accelrys' package Amorphous Cell Builder [19]. In all simulations, the periodic boundary conditions are applied in all three directions perpendicular to the faces of the cells.

2.3. Forcefields

All the calculations carried out in the present work are done using the PCFF forcefield [20] and its recent modification called NJPCFF forcefield [21] that enable computation of the interactions between ions and atoms/molecules. The PCFF forcefield contains 11 intra-molecular bonding terms such as a single-bond stretching term, a two-bond angle term, a dihedral middle-bond torsion term, etc. In addition, the forcefield includes two intra- and inter-molecular non-bonding (van der Waals and Coulomb) terms. Within the NJPCFF forcefield, S–O⁻ bond stretching and ⁻O–S–O⁻ two-bond angle parameters are defined for the PEO sulfonic acid dianion. In addition, a proton particle is introduced with a mass of 1.00797u (*u* is the atomic mass unit), a charge *q*

normalized by the electronic charge *e* of 1.0, and the van der Waals non-bonding parameters $r_i^* = 2.5$ and $\epsilon_i = 0.013$.

2.4. Selection of the initial configurations

For each of the 150 configurations of the three types of cells described in Section 2.2, the energy is initially minimized for 10,000 steps using the steepest-descent molecular-mechanics method. During these and the subsequent calculations, the Cell Multipole summation method with a relative dielectric constant of 1.0 and an update width of 1 Å is used when dealing with the non-bonding (van der Waals and Coulomb) interactions. Ten configurations for each of the three cells with the lowest energies are selected for the subsequent analysis. The energy of the selected cells is next minimized using a combination of the steepest-descent and the conjugate-gradient methods until a convergence defined by the maximum molar energy derivative of 10 kcal/(mole Å) is reached.

The resulting atomic configurations are next subjected to the standard molecular dynamics simulations for 1000 ps

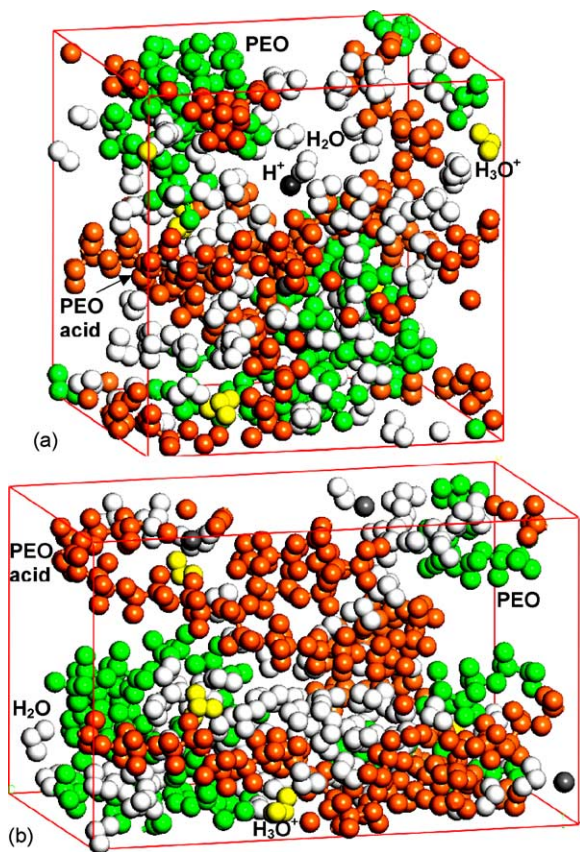


Fig. 2. An example of the computation cell containing the PEO polymer with the polymerization index of 40 in the: (a) original configuration; and (b) in the deformed state.

with a fixed time increment of 1 fs. The configurations are treated as NVT ensembles within which the temperature is held at 298 K using the Anderson thermostat method [22]. The Cell Multipole summation method with a relative dielectric constant of 1.0 and an update width of 1 Å is again used to efficiently handle the non-bonding interactions.

The molecular statics (energy minimization) and the molecular dynamics simulations described above are carried using the Accelrys' software package discover [23]. An example of the initial cell of type A is given in Fig. 2(a).

2.5. Vibrational spectral analysis

A comparison of the computed and measured vibrational spectra is generally used to validate the forcefield used in molecular modeling. The vibrational spectrum of a molecule can be calculated using the local mode method. Within this method, low-velocity components of the constituent particles are calculated using the classical molecular dynamics simulations. To calculate the fast vibrations of the atoms, on the other hand, several representative "equilibrium" atomic configurations are first generated using molecular dynamics simulations. For each of these configurations, the molecular vibrational frequencies are then determined using quantum mechanical calculations within which each particle is treated

as a quantum oscillator embedded in an effective medium of the remaining atoms. The local potential energy function for such an effective medium, V^{eff} , is defined as the following polynomial:

$$V^{\text{eff}}(Q) = K_0 + K_2 Q^2 + K_3 Q^3 + K_4 Q^4 \quad (1)$$

where Q defines coordinates of the species resulting from the molecular dynamics simulation runs.

Next, the following one-dimensional Schrödinger equation is solved:

$$\frac{\hbar}{2M} \left[\frac{d^2}{dQ^2} + V^{\text{eff}}(Q) \right] \Psi(Q) = E\Psi(Q) \quad (2)$$

where M is the standard (molecular geometry) G matrix in a normal mode analysis [26] and $\Psi(Q)$ is the wave function. The accuracy of the frequencies calculated using the local mode method is generally considered to be around 100 cm^{-1} .

2.6. Conformational and structural analyses

To characterize the intra-molecular and the inter-molecular structures of the materials studied in the present work, the following quantities are computed and analyzed: (a) pair correlation functions; (b) coordination numbers; (c) radii of gyration; (d) end-to-end molecular distances; (e) characteristic molecular ratio.

2.6.1. Pair correlation functions

Pair correlation functions (often referred to as radial distribution functions), $g_{x...z}(r)$, define the probability of finding a pair of atoms (labeled as x and z) at distance r apart, relative to the corresponding probability in the same material (at the same density), but under the condition of a completely random distribution of the particles [24].

2.6.2. Coordination number

The coordination number for particle z , $n_{x...z}(r)$, can be calculated from the corresponding pair correlation functions as:

$$n_{x...z}(r) = 4\pi \frac{N_z}{\langle V \rangle} \int_0^r g_{x...z}(s) s^2 ds \quad (3)$$

where $n_{x...z}(r)$ represents the number of x particles located within a sphere centered at the particle z and having a radius r , N_z is the total number of z particles in the system, while $\langle V \rangle$ is the average system volume.

2.6.3. Radius of gyration

The size of a polymer chain can be represented using its radius of gyration whose radius, R_g^2 , is defined as an average square distance of the constituent particles of the molecule from the molecule's center of gravity. The radius of gyration

can hence be expressed as:

$$R_g^2 = \frac{1}{N} \sum_{i=1}^N \langle (\mathbf{R}_i - \mathbf{R}_G)^2 \rangle \quad (4)$$

where N is the number of constituent particles, \mathbf{R}_i the position vector of particle i , $\langle \rangle$ denotes an average and the center of gravity position vector is defined as:

$$\mathbf{R}_G = \frac{1}{N} \sum_{i=1}^N \mathbf{R}_i \quad (5)$$

A simple manipulation of Eqs. (4) and (5) yields:

$$R_g^2 = \frac{1}{N^2} \sum_{i=1}^{N-1} \sum_{j=n+1}^N \langle (\mathbf{R}_i - \mathbf{R}_j)^2 \rangle \quad (6)$$

2.6.4. The mean square end-to-end molecular distance

An alternative measure of the size of a polymer chain is the mean square end-to-end distance, $\langle R^2 \rangle$. This measure of the molecule size (as well as the characteristic ratio, C_n) takes into account the short-range interactions (as manifested, for instance, by the rotational isomerism, the torsional chain stiffness, etc.) between various segments of a molecular chain. The mean square end-to-end distance is defined as:

$$\langle R^2 \rangle = \langle \mathbf{R}_M - \mathbf{R}_1 \rangle^2 \quad (7)$$

where the subscripts M and 1 are used to denote the last and the first particle in the backbone of a molecular chain.

2.6.5. Characteristic ratio

The chain dimensions can also be described (strictly speaking only in the limit of infinitely long chains) using the following characteristic ratio C_n [24]:

$$C_n \equiv \frac{\langle R^2 \rangle}{\sum_{i=1}^{M-1} l_i^2} \quad (8)$$

where l is the bond length and $M-1$ the number of bonds along the backbone of the molecule.

In the absence of short-range interactions between different segments of a chain, the mean square end-to-end length of a chain is defined, in accordance to the random-walk process, by the denominator on the left hand side in Eq. (8). Hence, C_n represents a ratio of the actual and the random-walk based mean square end-to-end chain lengths.

2.7. Transport properties analysis

When the mass or the ionic transport properties of the solid polymer electrolytes are considered in membrane applications, three fundamental phenomena must be analyzed: (1) adsorption of the transported species onto the membrane; (2) their transport through the membrane; (3) desorption of

the transported species from the opposite surface of the membrane. However, it is well established that transport through the membrane is the slowest and, hence, the rate controlling process [25].

Within an atomistic-modeling framework, the diffusion coefficient for species α , D_α , can be defined by the following equation [24]:

$$D_\alpha = \frac{1}{6N_\alpha} \lim_{t \rightarrow \infty} \frac{d}{dt} \sum_{i=1}^{N_\alpha} \langle [R_i(t) - R_i(0)]^2 \rangle \quad (9)$$

The sum on the right side of Eq. (9) divided by N_α represents the mean square displacement (MSD) of species α , N_α is the number of diffusing α particles, t time and $R_i(t)$ is the radial displacement of particle i of species α at time t . It must be noted that Eq. (9) pertains to the so-called Einstein-diffusion and, hence, is valid only when diffusion of the particles is a random walk process, i.e. the displacement of a particle at some time is uncorrelated with its displacement at any previous or future time. In this regime of diffusion, there is a linear relation between the mean square displacement and the time. When the polymer-chain surrounding of a diffusing particle inhibits free movement of such particle, i.e. the particle is confined (at least temporarily) to a small space, the mass-transport process is called an anomalous-diffusion. In this case $\langle [R_i(t) - R_i(0)]^2 \rangle \propto t^n$, where $n < 1$, and Eq. (9) is not applicable. When $n > 1$ in the $\langle [R_i(t) - R_i(0)]^2 \rangle \propto t^n$ relation, on the other hand, the mass-transport is dominated by a non-diffusion process. For instance, when $n = 2$, the particle transport takes place by the so-called free-flight process in which particles move in a low-density medium without any interactions with the medium. To identify the portion of the simulation runs within which the Einstein-diffusion is the dominant mass-transport mechanism, a $\log(\text{MSD})$ versus $\log(t)$ plot should be generated and the slope of this curve compared with unity.

When the Einstein-diffusion regime is reached, the ionic conductivity, σ , can be determined using the following Einstein equation:

$$\sigma = \frac{e^2}{6t \langle V \rangle kT} \left(\sum_i Z_i^2 \langle [R_i(t) - R_i(0)]^2 \rangle + 2 \sum_{j>i} Z_i Z_j \langle [R_i(t) - R_i(0)][R_j(t) - R_j(0)] \rangle \right) \quad (10)$$

where e is the electronic charge, Z the valence, k the Boltzmann constant and T is the temperature. The first term on the right-hand side of Eq. (10) represents the sum over all ionic mean square displacements weighted by the ionic charges while the second term is the sum of correlations of the ionic displacements and describes the contribution of the electrostatic interactions to ionic conductivity.

2.8. Strength analysis

When the PEO sulfonic acid-based solid electrolytes are used in thin membrane applications, they must generally satisfy not only high ionic-conductivity requirements, but also meet strength requirements in order to ensure a long life cycle. To assess the level of strength in the PEO sulfonic acid-based materials analyzed in the present work, classical molecular dynamics calculations are employed using the Accelrys' program discover [23]. The molecular dynamics procedure utilized involves the following steps:

- The atomic/molecular structure in the initial (cubic, undeformed) cell is first equilibrated by treating the particles in the cell and the cell itself as an NPT ensemble, where N is the number of particles, P the pressure and T the absolute temperature. During this procedure, the initial particle positions and the (cubic) cell edge length are adjusted to keep the pressure constant and equal to its target value (the atmospheric pressure of 0.1 MPa in the present case). The Anderson method for pressure control [23] which allows a change in the cell volume but not in its shape is used in this step of the molecular dynamics simulations.
- $N\sigma T$ molecular dynamics simulations (where σ is the stress tensor) are next utilized within which tensile (normal) stress is applied in one direction at a constant rate of 1 bar/ps while the remaining two normal stresses are kept at their 0.1 MPa level. In addition, all shear stresses are kept at a zero level. The magnitude of the resulting longitudinal (normal) strain is then monitored during loading and used to construct the tensile stress-strain curve.
- The procedure in (b) is continued until "plastic" yielding associated with an abrupt increase in the longitudinal strain rate is observed.

An example of the deformed cell of type A is given in Fig. 2(b).

Table 1

Computed vibrational absorption frequencies in cm^{-1} for the PEO sulfonic acid dianion in vacuum and water, and computed and measured [3,16–20] vibrational frequencies for PEO sulfonic acid

Row	PEO sulfonic acid dianion		PEO sulfonic acid (measured)	Dominant bond assignment
	In vacuum (computed)	In water (computed)		
1		3670	3710	O–H in water, intra-molecular
2	3500	3520	3400–3600	O–H in H_3O^+ , hydrogen bond
3		3550	3400–3600	O–H in PEO/water
4	2930	2850	2925	C–H
5	1250	1270	800–1350	C–C
6	1230	1250	1100	C–O
7			1120–1170	S=O
8			850–910	S–O
9		1100	600–700	$\text{SO}_3^- \text{H}_3\text{O}^+$
10	1020	1100	1070–1140	S–O ⁻
11	1090	1090	1070–1100	C–S

3. Results and discussion

3.1. Vibrational spectral analysis

To validate the NJPCFF forcefield used in the present work, the local mode method discussed in Section 2.5 is applied to an isolated PEO sulfonic acid dianion in vacuum and in water. The results obtained are compared with their available corresponding experimental counterparts for the PEO sulfonic acid (as originally compiled by Ennari et al. [10–17]) and a summary of this comparison is given in Table 1. Based on the results displayed in Table 1, the following main findings can be established:

- The computed vibrational frequencies for the sulfonic acid group in PEO sulfonic acid dianion in vacuum (1020 cm^{-1}) and in water (1100 cm^{-1}) listed in Row 10 are quite close to their experimental counterparts ($1040\text{--}1090 \text{ cm}^{-1}$), considering the fact that the accuracy of the local mode method is about 100 cm^{-1} . This finding suggests that the additional bonding and non-bonding forcefield parameters added to the NJPCFF to account for the polymer/ion interactions correctly account for the atomic-level dynamics of the sulfonic end groups in the PEO sulfonic acid dianions.
- The computed and measured frequencies cited in (a) are clearly different than the measured ($850\text{--}910 \text{ cm}^{-1}$) frequency for the S–O bond stretch (Row 8), and are also different than the measured (1160 cm^{-1}) frequency for the S=O bond stretch in the PEO sulfonic acid, Row 7.
- Since the difference in the S–O⁻ bond stretch frequencies in the PEO sulfonic acid in vacuum and in water (Row 10) are within the range of accuracy for the local mode method, no definite conclusion can be drawn regarding the effect of the surrounding medium on the atomic-level dynamics of the sulfonic acid end group in the PEO sulfonic acid dianions.
- A comparison of the remaining computed and experimental frequencies shown in Table 1 indicates that, in general, NJPCFF predicts quite accurately the atomic-

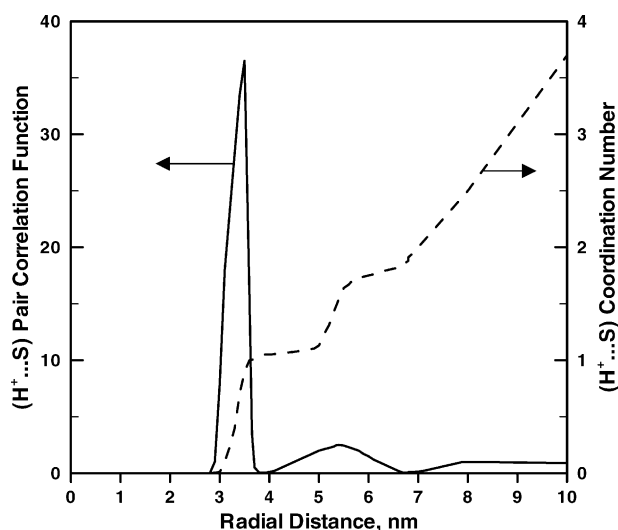


Fig. 3. Radial dependence of the pair correlation function between the proton (H^+) and the sulfur atom (S) in the PEO sulfonic acid dianion and of the corresponding coordination number for the same type of particles.

level dynamics of the PEO sulfonic acid and of the PEO sulfonic acid dianions.

3.2. Pair correlation and coordination number analyses

The coordination between different types of particles is studied by analyzing the corresponding pair correlation functions $g(r)$ and the associated coordination numbers $n(r)$ in the first and, when available, in the second solvation shells. An example of the pair correlation function versus the particles separation distance plot is given in Fig. 3. A summary of the results of the coordination analysis is given in Table 2. These results can be interpreted as follows:

- The proton...ether-oxygen (oxygen in the backbone of the PEO sulfonic acid and the PEO polymer chains) correlation function and the single solvation-shell coordination number decrease slightly while the corresponding solvation-shell radius increases slightly, from cell type A to cell type C, Row 1. This finding can be related to the number of water molecules in the cell and suggests
- that the H^+ and ether-O particles tend to become more separated and less coordinated by the introduction of additional water molecules. Due to the large dielectric constant of water and the observed increased $H^+ \cdots$ ether-O separation distances in the B and C types of cells, the non-bonding (Coulomb and van der Waals) interactions are expected to decrease when the material at hand is hydrated.
- An increased number of water molecules in the B and C types of cells also appears to reduce slightly the coordination number of protons within the first solvation-shell of sulfur atoms in the sulfonic acid end groups of the PEO sulfonic acid dianions and to increase slightly the solvation-shell radius, Row 2. This effect is, however, much less pronounced in the case of the second solvation-shell.
- Two well-defined solvation shells of water molecules (denoted by their oxygen atom, O2) around protons with comparable respective radii and comparable respective coordination numbers in the three types of cells are observed, Row 3. This finding suggests that protons are mainly found in water-rich regions located at relatively large distances from the PEO sulfonic acid dianions and the PEO polymer molecular chains. Hence, protons are expected to be quite mobile in the presence of water in the materials at hand, and consequently, the contribution of the hopping mechanism to proton transport is expected to be significant.
- Coordination between ether-oxygen and oxygen (named O3) in the hydronium ions, Row 4, is seen to result in the formation of a strong second solvation-shell whose strength and the radius seem to increase slightly as the number of water molecules increases from cell type A toward cell type C. This finding suggests that ether-oxygen atoms and hydronium ions are separated by water molecules, and that the separation distance increases with the number of water molecules present in the system.
- An increase in the number of water molecules in cells B and C gives rise only to a slight increase in the radius of the first solvation-shell for hydronium ions surrounding the sulfur atom in the sulfonic acid end group, Row 5. The corresponding coordination number, however,

Table 2

The results of the pair correlation and the coordination number analyses carried out in the present work

Row number	Pair correlation function	Cell A		Cell B		Cell C	
		Radius (Å)	Coord. number	Radius (Å)	Coord. number	Radius (Å)	Coord. number
1	$H^+ \cdots$ ether-O	2.44	2.05	2.51	1.91	2.55	1.90
2	$H^+ \cdots$ S	3.54 (6.10)	2.0 (2.32)	3.59 (6.07)	1.79 (2.40)	3.6 (6.11)	1.75 (2.09)
3	$H^+ \cdots$ O2	2.41 (4.91)	2.95 (8.25)	2.45 (5.25)	2.66 (9.11)	2.56 (4.99)	2.67 (8.72)
4	$O3 \cdots$ ether-O	3.42 (4.52)	0.41 (2.95)	3.51 (4.69)	0.40 (3.17)	3.54 (4.81)	0.35 (3.19)
5	$O3 \cdots$ S	4.13 (6.31)	1.21 (2.09)	4.18 (6.49)	1.25 (2.00)	4.19 (6.58)	1.12 (1.95)
6	$O2 \cdots$ O3	3.15	7.95	3.29	8.51	3.49	8.49
7	$O2 \cdots$ ether-O	3.42 (4.12)	1.09 (2.12)	3.49 (4.19)	1.02 (1.80)	3.59 (4.30)	1.01 (1.59)
8	$O2 \cdots$ S	4.12 (5.96)	10.62 (16.32)	4.22 (6.22)	10.52 (15.99)	4.63 (6.12)	10.54 (16.92)

The number within parenthesis pertain to the second solvation-shell. O2: oxygen atom in H_2O ; O3: oxygen atom in H_3O^+ .

while being affected by the number of water molecules in the cell, varies with this number in a more complex manner. A slightly larger effect of hydration is seen in the case of the second solvation-shell.

- (f) Water molecules form a strong single solvation-shell around the hydronium ions and, while the strength of this solvation-shell clearly varies with the number of water molecules in the cell, Row 6, the nature of this interaction appears to be quite complex.
- (g) In the case of all three types of cells, water molecules are strongly correlated with the ether–oxygen atoms which results in the formation of two well-defined H₂O solvation shells, Row 7. The radii and the coordination numbers of these shells, however, are not significantly affected by differences in the number of water molecules between the three types of cells.
- (h) Water molecules are strongly correlated with sulfur atoms in the sulfonic acid end groups resulting in the formation of two well-defined solvation shells of H₂O molecules, Row 8. It is generally believed (e.g. [27]) that at least 10 water molecules should be correlated with each sulfonic acid end group in order to obtain good ionic conductivity in the PEO sulfonic acid-based solid polymer electrolytes. Based on the water-sulfur correlation data listed in Row 8, Table 2, one can expect that the materials associated with all three types of cells are ionically conductive.

3.3. Conformation analysis

The structure of the PEO sulfonic acid dianion and PEO polymer chains is studied by analyzing the distributions of the OSCC, SCCC, CCCO, CCOC and OCCO dihedral angles. The dihedral-angle for a chain of three linearly-connected bonds where the bonds are represented with vectors r_{i-1} , r_i and r_{i+1} , respectively, is the angle between the plane of the vectors r_{i-1} and r_i , and the plane of the vectors r_i and r_{i+1} . A typical (SCCC) dihedral-angle distribution plot is shown in Fig. 4. The chain conformations associated with a dihedral-angle of 0° are referred as the *trans* (T) conformation states while those associated with dihedral angles of -120° and 120° are denoted as the *gauche minus* (G⁻) and the *gauche plus* (G⁺) conformation states, respectively, is shown in Fig. 4.

A summary of the dihedral-angle results obtained in the present work is given in Table 3. To enable a simple quantitative comparison of the populations of the three dihedral-angle conformation states (T, G⁺ and G⁻) in the three types of cells, the T conformation state is taken to correspond to a -60° to 60° dihedral-angle range, the G⁻ conformation state to a -180° to 60° dihedral-angle range while the G⁺ conformation state to a 60°–180° dihedral-angle range. Due to torsional symmetry of the PEO sulfonic acid dianion and the PEO molecules, the G⁻ and G⁺ conformation states are generally found to be present with approximately equal probabilities for each of the five dihedral angles analyzed. Therefore, in Table 3, only the percentages of the T conformation

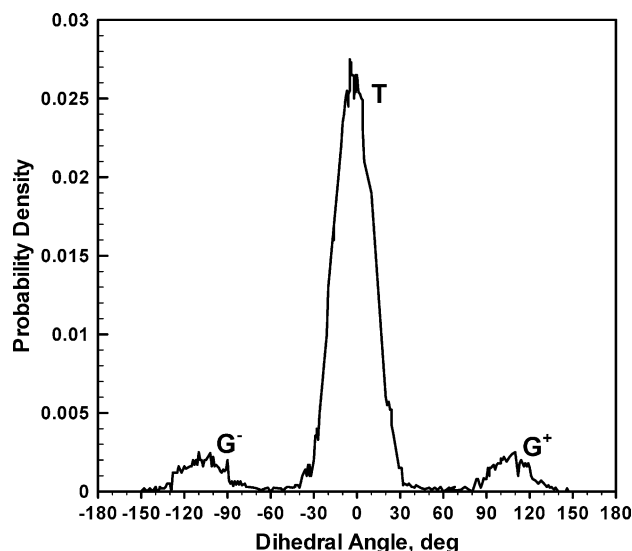


Fig. 4. Probability density plot for the average SCCC dihedral-angle for the PEO sulfonic acid dianion.

state for the five dihedral angles are given. The corresponding percentages of the G⁻ and the G⁺ conformation states can be readily computed.

The results displayed in Table 3 can be summarized as follows:

- The mean values for the corresponding five dihedral angles are very similar in the three types of cells and, thus, not significantly affected by the existing differences between the three types of cells in the amount of PEO polymer and the number of water molecules.
- The T, G⁻ and G⁺ conformation states of the OSCC dihedral-angle are almost equally populated which is most likely the result of symmetry of the PEO sulfonic acid dianion end groups.
- The SCCC dihedral-angle is almost completely populated with the *trans* conformation state.
- The T, G⁻ and G⁺ conformation states for the CCCO dihedral-angle are nearly equally populated.
- The conformation of the CCOC dihedral-angle is dominated by its T state although the G⁻ and the G⁺ conformation states are present in measurable quantities.
- The *trans* state of the OCCO dihedral-angle is deficient (i.e. its fraction is smaller than 33%) indicating the occurrence of the so-called *gauche* effect. This effect is gener-

Table 3

Mean values of the percent of the *trans* conformation state in various dihedral angles in the PEO sulfonic acid-based polymeric electrolyte studied in the present work

Dihedral-angle	Cell A	Cell B	Cell C
OSCC	32.8	34.1	33.8
SCCC	94.1	95.0	93.3
CCCO	34.0	32.1	33.7
CCOC	82.2	85.8	84.7
OCCO	30.1	27.4	28.3

ally promoted by high polarity, high dielectric constant and the presence of hydrogen bonding in the surrounding medium and all these conditions are present in the material at hand [14]. In polymers with a pronounced gauche effect, a new cation transport mechanism is often observed in which the cations hop from one ether–oxygen to the adjacent one. However, such a mechanism is not expected to play a major role in material analyzed in the present work considering the fact that no significant correlation is found between the cations (protons and hydronium ions) and the ether–oxygen atoms residing in the backbone of PEO sulfonic acid and the backbone of PEO molecules.

It should be noted that the results displayed in Table 3 reveal that the number of water molecules in the computational cell does not have a major effect on the population distribution of various dihedral angles, and that the variations observed are a reflection of the statistical nature of the problem at hand.

3.4. Dimensional analysis

To get a further insight into the conformation of the PEO sulfonic acid dianions in the three cells, Eqs. (6)–(8) are used to compute the radius of gyration, the end-to-end distance and the characteristic ratio for the PEO sulfonic acid dianions in the three types of cells. The results of this calculation are given in Table 4 and can be summarized as follows:

- The mean values of the corresponding dimensional parameters do not differ significantly in the three types of cells.
- The mean values for the radius of gyration and for the end-to-end distance in all three types of cells are smaller by a factor of approximately 60% than their counterparts for PEO sulfonic acid dianions in vacuum [14]. This finding suggests that these dianions are more curved or coiled in the three cells studied in the present work and more extended when present as isolated molecules in vacuum. At least two reasons may be cited for the observed change in the PEO sulfonic acid dianion conformations: (i) due to a high value of the dielectric constant of water, the repulsion between the two negatively charged ends of the PEO sulfonic acid dianions is reduced in the case of the three types of cells analyzed in the present work. This enables the dianions ends to get closer to each other; and (ii) the observed gauche effect results naturally in the chains with lower values of their radius of gyration and of their end-to-end distance.

Table 4
Average values and standard deviations for the radius of gyration, the end-to-end distance and the characteristic ratio for the PEO sulfonic acid dianions in the three cells studied in the present work

Dimensional parameter	Cell A	Cell B	Cell C
Radius of gyration (\AA)	6.22 ± 0.14	5.98 ± 0.22	6.11 ± 0.25
End-to-end distance (\AA)	12.3 ± 3.4	11.9 ± 4.4	12.5 ± 3.3
Characteristic ratio (N/A)	3.2 ± 0.1	3.3 ± 0.1	3.0 ± 0.1

Table 5

The average values (in $10^{-9} \text{ m}^2/\text{s}$) and the standard deviations for the diffusion coefficient of various species in the PEO based hydrated solid electrolyte studied in the present work

Diffusing species	Cell A	Cell B	Cell C
H^+	0.36 ± 0.04	0.46 ± 0.05	0.53 ± 0.04
H_3O^+	0.39 ± 0.04	0.45 ± 0.06	0.50 ± 0.07
H_2O	0.82 ± 0.06	0.86 ± 0.07	0.92 ± 0.10
O^-	0.03 ± 0.02	0.04 ± 0.02	0.04 ± 0.01
Ether–O	0.02 ± 0.01	0.02 ± 0.01	0.02 ± 0.01

- The values for the characteristic ratio listed in Table 4 are also lower than their counterparts for the isolated PEO sulfonic acid dianions in vacuum ($C_n = 9.4$, [14]) confirming the observation made above that hydration makes these ions less extended.

It should be noted that the results presented in Table 4 suggest that the radius of gyration, the end-to-end distance and the characteristic ratio are not significantly affected by the number of water molecules in the cell, as evidenced by relatively small changes in the magnitudes of these quantities due to an increase in the number of water molecules compared with the standard deviation values at a given number of water molecules.

3.5. Mass and charge transport properties

Diffusion coefficients for the proton, the hydronium ion, the water, the oxygen in the sulfonic acid end group and the ether–oxygen of the PEO sulfonic acid and PEO polymer chains for the three types of cells computed using Eq. (9) are summarized in Table 5. The condition for the Einstein-diffusion discussed in Section 2.7 was met in the case of all particles in all three types of cells. The results displayed in Table 5 can be briefly summarized as follows:

- The diffusion coefficients of the proton, the hydronium ion and the water are mutually comparable in the case of each of the three types of cells. The diffusion coefficients of the oxygen ion in the sulfonic end group and of the ether–oxygen in the backbone of the PEO sulfonic acid and the PEO polymer chains are smaller by at least an order of magnitude. This finding can be readily understood considering the fact that H^+ , H_3O^+ and H_2O are small free particles while O^- and ether–O are covalently-bonded constituents of the PEO sulfonic acid dianion chains while ether–O is also a constituent of the PEO molecular chains.
- In all three types of cells, the diffusion coefficient of water is the highest and increases slightly with the number of water molecules in the cell. While this finding can be partly attributed to a relatively large (40 wt.%) weight percent of H_2O in the system, it may also suggest that the other two small particles, i.e. H^+ and H_3O^+ cations, are involved in non-bonding interactions with the PEO sul-

fonic acid dianions and the PEO molecules which lowers their diffusivities.

- (c) As the number of water molecules increases from the cell type A to the cell type C, the diffusion coefficients of H^+ , H_3O^+ and H_2O all increase. Between the two cations, the diffusion coefficient of H^+ increases at a somewhat faster rate than that of H_3O^+ as the number of water molecules is increased. This finding suggests that as the number of water molecules increases, the role of the proton hopping mechanism in the H^+ transport and, hence, the magnitude of the ionic conductivity increase.
- (d) Since the diffusion coefficients of O^- and of ether-O are substantially lower than those of H^+ and H_3O^+ , the latter particles appear, for the most part to be free to move through the material as opposed to being confined by or bonded to and moving with the PEO sulfonic acid dianion and the PEO molecular chains.

The total ionic conductivity computed using Eq. (10) are: 6.4, 6.9 and 7.2 mS/cm for the cell types A, B and C, respectively. The standard deviation for these results is around 0.8 mS/cm. For comparison, the corresponding experimental values obtained using impedance measurements are 1.5 and 0.015 mS/cm at the relative humidity levels of 75.3 and 38.2%, respectively [8]. While the information provided in Ref. [8] does not enable determination of the corresponding water weight percents in the solid polymer electrolyte, the computed values appear to be somewhat higher than expected. One possible explanation for this shortcoming of the model is the way in which the proton hopping mechanism was modeled. That is, proton hopping between adjacent water molecules is assumed to take place without breaking of the chemical bonds, the process which is generally associated with a large activation energy and, hence, a lower rate. Consequently, the computed contribution of proton hopping to the ionic conductivity in the material at hand is expected to be somewhat overestimated.

By analyzing separately the contributions of the protons and the hydronium ions to the ionic conductivity of the material at hand, it is established that in all three types of cells these two contributions are comparable. However, as the number of water molecules is increased from Cell A toward Cell C, the relative contribution of the proton hopping mechanism to the ionic conductivity increases.

3.6. Mechanical strength analysis

The average tensile stress-strain curves along with the corresponding one-standard deviation error bars generated using the procedure described in Section 2.8 for the three types of cells are shown in Fig. 5. The corresponding experimental stress-strain curve for a 40 wt.% hydrated PEO polymer [28] is also shown in Fig. 5 for comparison. The results displayed in Fig. 5 can be summarized as follows:

- (a) Despite a considerable scatter in the simulation results, the computed tensile stress-strain curves for the materials

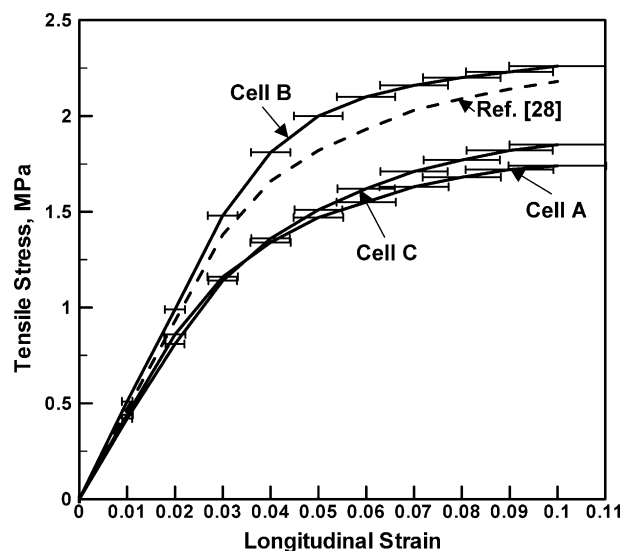


Fig. 5. Experimental stress-strain curve for a 40 wt.% hydrated PEO polymer [28] and computed stress-strain curve for the three types of cells containing PEO sulfonic acid solid polymer electrolyte.

associated with the three types of cells are surprisingly quite close to the experimental curve.

- (b) In spite of a significant value of the standard deviation for the longitudinal strain in the three types of cells, material associated with the cell type B is found to possess statistically the largest value of its yield strength. This finding suggests that at a same level of hydration, there may be an optimum fraction of the PEO polymer which gives the best combination of ionic conductivity and strength in the PEO sulfonic acid-based solid polymer electrolyte. This conjunction will be explored in more details in the future work.
- (c) A detailed examination of the conformations of the PEO sulfonic acid dianions and of the PEO polymer molecules reveals that numerous gauche-to-trans conformation-state transitions in the OCCO dihedral-angle take place during yielding. Consequently, the mean values of the percent of the trans conformation state in the three types of cells at a strain level of 10% are found to be in a 39.6–43.2% range. This values are substantially higher than their counterpart (27.4–30.1%, Table 3) in the initial state. The gauche-to-trans conformation-state transitions, thus, appear to be the primary yielding mechanism in the material under investigation.

4. Conclusions

Based on the results obtained in the present work, the following main conclusions can be drawn:

1. Molecular modeling, in conjunction with experimental investigations, can be a very instrumental tool in identifying the microstructural features and the atomic-level mech-

anisms which control various physical and mechanical properties of solid polymer based electrolytes.

2. In PEO sulfonic acid dianion based solid polymer electrolytes, both the classical cation diffusion and a proton hopping mechanism play important roles in the ionic conduction.
3. As expected, hydration promotes ionic conductivity but degrades the strength of the PEO sulfonic acid solid electrolytes.
4. At a fixed level of hydration, it appears that there is an optimum level of the PEO polymer content which gives the best combination of the material ionic conductivity and strength.

Acknowledgements

The material presented in this paper is based on work supported by the U.S. Army Grant No. DAAD19-01-1-0661. The authors are indebted to Dr. Bonnie Gersten, Fred Stanton and William DeRosset of ARL for the support and a continuing interest in the present work.

References

- [1] M. Armand, J. M. Chabagno, M. Duclot, Second International Meeting on Solid Electrolytes, St Andrews, UK, September 20–22, 1978. Raman Spectroscopy, Academic Press, New York, 1964, pp. 310.
- [2] J.M.G. Cowie, *Polym. Int.* 47 (1998) 20.
- [3] B. Scrosati, *Polym. Int.* 47 (1998) 50.
- [4] S.A. Hashmi, R.J. Latham, R.G. Linford, W.S. Schindwein, *Polym. Int.* 47 (1998) 28.
- [5] H.R. Allcock, N.J. Sunderland, R. Ravikiran, J.M. Nelson, *Macromolecules* 31 (1998) 8026.
- [6] K.D. Kreuer, *Chem. Mater.* 8 (1996) 610.
- [7] S. Gottesfeld, T.A. Zawodzinski, in: R.C. Alkire, H. Gerischer, D.M. Kolb, C.W. Tobias (Eds.), *Advances in Electrochemical Science and Engineering*, 5, Wiley-VCH, Weinheim, 1997, p. 197.
- [8] J. Herranen, J. Kinnunen, B. Mattsson, H. Rinne, F. Sundholm, L. Torrel, *Solid State Ionics* 80 (1995) 201.
- [9] M. Eikerling, A.A. Kornyshev, U. Stimming, *J. Phys. Chem. B* 101 (1997) 10807.
- [10] J. Ennari, J. Hamara, F. Sundholm, *Polymer* 38 (1997) 3733.
- [11] J. Ennari, M. Elomaa, F. Sundholm, *Polymer* 40 (1999) 5035.
- [12] J. Ennari, I. Neelov, F. Sundholm, *Comput. Theor. Polym. Sci.* 10 (2000) 403.
- [13] J. Ennari, M. Elomaa, I. Neelov, F. Sundholm, *Polymer* 41 (2000) 985.
- [14] J. Ennari, I. Neelov, F. Sundholm, *Polymer* 41 (2000) 4057.
- [15] J. Ennari, I. Neelov, F. Sundholm, *Polymer* 41 (2000) 2149.
- [16] J. Ennari, I. Neelov, F. Sundholm, *Polymer* 42 (2001) 8043.
- [17] J. Ennari, L.O. Pietila, V. Virkkunen, F. Sundholm, *Polymer* 43 (2002) 5427.
- [18] http://www.accelrys.com/mstudio/ms_modeling/visualizer.html.
- [19] http://www.accelrys.com/mstudio/ms_modeling/amorphous.html.
- [20] H. Sun, *J. Comp. Chem.* 15 (1994) 752.
- [21] J. Ennari, Ph.D Thesis, University of Helsinki, 2000, ISBN 951-45-9140-2, <http://ethesis.helsinki.fi/julkaisut/mat/kemia/vk/ennari>.
- [22] *Polymer User Guide, Part 1*, Biosym Technologies, San Diego, CA, 1993, pp. 3–12.
- [23] http://www.accelrys.com/mstudio/ms_modeling/discover.html.
- [24] M.P. Allen, D.J. Tildesley, *Computer Simulation of Liquids*, Clarendon Press, Oxford, 1987.
- [25] P.F. Flory, *Statistical Mechanics of Chain Molecules*, Wiley, New York, 1969.
- [26] *Polymer 3.0.0, Polymer Modeling Software, User Guide, Part 1*, MSI, San Diego, October 1995, pp. 3–16.
- [27] S. Hietala, S. Homberg, J. Nasman, D. Ostrovskii, M. Paronen, R. Serimaa, F. Sundholm, L. Torell, M. Torkkeli, *Angew. Makromol. Chem.* 253 (1997) 151.
- [28] H.Z. Geng, R. Rosen, B. Zheng, H. Shimoda, L. Fleming, J. Liu, O. Zhou, *Fabrication and properties of composites of poly(ethylene oxide) and functionalized carbon nanotubes*, *Adv. Mat.* 2004, in press.